DOI: 10.1002/cbic.200900196

NMR Spectroscopic Characterization of the Adenine-Dependent Hairpin Ribozyme

Janina Buck,[a] Yan-Li Li,[b, c] Christian Richter,[a] Jacques Vergne,[b] Marie-Christine Maurel,*[b] and Harald Schwalbe*[a]

Time-resolved NMR spectroscopy was applied to study ribozyme-mediated RNA catalysis in a mutant of the hairpin ribozyme, the adenine-dependent hairpin ribozyme (ADHR; M. Meli, et al. *J. Biol. Chem.* **2003**, *278*, 9835–9842) with atomic resolution. The mutant ADHR was designed to investigate the role of cofactors in RNA catalytic mechanisms in order to understand cellular processes that could have been present in the archaic "RNA world" and of their evolution towards functional RNAs in modern cellular processes, as for example, found in the *glmS* ribozyme. Conformational changes due to RNA cleavage were analyzed following spectral changes of the NMR imino proton resonances that could be assigned both for the pre- and postcleaved conformation for this 80-nucleotide long RNA. ^{31}P NMR spectroscopic studies allowed us to confirm the formation of a cyclic phosphodiester as a result of the cleavage process. For ADHR, both metal ions and the cofactor adenine are essential for self-cleaving activity. The interaction of the ribozyme with the cofactor adenine is found to be transient and too weak to significantly change the RNA structure or to modulate the spectroscopic characteristics of the cofactor. ADHR therefore represents a ribozyme in which high activation barriers have to be overcome to populate cleavage-competent states that exhibit short life times. We show that conformational dynamics, but not the chemistry, constitute the rate-limiting step in catalysis of the adenine-dependent hairpin ribozyme.

Introduction

The structures and functions of RNAs are remarkably diverse. The diverse roles of RNAs in all living cells and the discovery of new functions collectively underline their importance in cellular mechanisms. Each cell contains RNAs in various forms, as short and long oligonucleotides, single- and double stranded, and endowed with multiple roles (informational, catalytic, serving as templates, guides, defense, etc.) and certain molecules perform several of these functions. Due to the phenotypic and genotypic behavioral roles, RNAs have been proposed to have constituted a prebiotic "RNA world",[2–4] which is speculated to have preceded the contemporary DNA–RNA–protein world.[5] Catalytic or regulatory RNA motifs, including ribozymes or riboswitches are discovered to be part of modern cellular processes and can perform their cellular function without help from any proteins. Viroids and other related RNA species, such as satellite RNAs, possess catalytic motifs that can perform and assist their own replication. The function of riboswitch elements in regulation is supposed to depend on an allosteric structural rearrangement in response to binding of a specific small-molecule metabolite. Furthermore, the *glmS* ribozyme is an example of a catalytic riboswitch, for which the mechanism of gene regulation relies on the specific cleavage of the RNA backbone. Thereby, cleavage is dependent on the small molecule cofactor glucosamine-6-phosphate (GlcN6P) that catalyses this chemistry.[6–8] Thus, we may learn about the origins and evolution of life as well as about modern cellular processes by studying RNA interactions with small molecules.

All small naturally occurring ribozymes found to date are thought to catalyze the cleavage of the RNA phosphodiester backbone following an identical chemical mechanism also utilized by the protein enzyme RNase A.[9] Cleavage of the RNA backbone follows a bimolecular nucleophilic substitution mechanism. Known ribozymes strongly differ in sequence and structure and include the hammerhead,[10,11] the hepatitis delta virus (HDV),[12,13] the Varkud satellite,[14,15] the hairpin,[16–19] and the *glmS*[8] ribozymes. Although they are involved in different cellular processes, such as processing of satellite, virus or viroid RNAs or controlling gene expression, they constitute evolutionary solutions evolved to perform the identical chemical reaction. In principle, ribozymes act autocatalytically and in a reversible manner to fulfill their biological functions. The detailed mechanism, however, of how ribozymes perform their catalytic

[a] *J. Buck, Dr. C. Richter, Prof. Dr. H. Schwalbe*
Institute for Organic Chemistry and Chemical Biology
Center for Biomolecular Magnetic Resonance
Johann Wolfgang Goethe-University, Max von Laue Strasse 7
60438 Frankfurt am Main (Germany)
Fax: (+49) 69-798-29515
E-mail: schwalbe@nmr.uni-frankfurt.de

[b] *Dr. Y.-L. Li, J. Vergne, Dr. M.-C. Maurel*
ANBioPhy, University Pierre & Marie Curie
4 Place Jussieu, 75252 Paris (France)
Fax: (+33) 144279916
E-mail: marie-christine.maurel@upmc.fr

[c] *Dr. Y.-L. Li*
Present address: Laboratory of Vascular Biology
Institute of Molecular Medicine, Peking University
New Life Science Building, 5 Yi He Yuan Road, Beijing (China)

Supporting information for this article is available on the WWW under http://dx.doi.org/10.1002/cbic.200900196 or from the author.

function, namely RNA cleavage and ligation, varies in different ribozymes. This variation is brought about by the contribution of different RNA residues that constitute the catalytic site of the respective ribozyme, and thus take part in active-site chemistry,[20,21] as well as by the participation of different essential cofactors. In the HDV ribozyme, for example, amongst others, a specifically bound Mg^{2+} is reported to participate in active-site chemistry[22] and the *glmS* ribozyme is reported to be active only in the presence of its cofactor GlcN6P.[8]

Amongst the catalytic RNA motifs, the hairpin motif of the tobacco ringspot virus satellite (TRSV) is of particular interest. The wild type (wt) hairpin ribozyme is composed of two domains each formed by an internal loop flanked with two helices, which come into close contact during catalysis.[23,24] The two domains form a four-way junction, although a minimal two-way junction also results in a functional ribozyme.[18]

In order to test the cofactor dependence of the wt-hairpin ribozyme, Maurel and co-workers have previously identified new active versions from inactive mutants that have recovered their activity by the addition of the exogenous cofactor adenine.[1] The nucleobase adenine is supposed to be a prebiotic compound, additionally it is central in cellular metabolism, for instance of AMP, ATP, FAD, NAD or CoA,[25] it is one of the four canonical nucleobases of DNA and RNA and it possesses catalytic properties by itself. In fact, transcriptional and translational regulation by adenine-dependent riboswitch elements are known.[26]

These new variants, the adenine-dependent hairpin ribozymes (ADHR), were selected in vitro in a systematic evolution of ligands by exponential enrichment procedure (SELEX). The secondary structure of ADHR ribozymes comprise the minimal wt-hairpin ribozyme with four helical regions (helices 1–4) that are separated by two loop regions (loops A and B). The two domains are connected by a short C-rich linker region. The RNA construct used in our NMR studies (ADHR1-nmr) comprised 80 nucleotides and was based on ADHR1 following the original nomenclature[1] (Figure 1). In construct ADHR1-nmr helices 1 and 4 are elongated by additional G–C base pairs and a stable UUCG tetraloop caps helix 4. The four mutations with respect to the wt-hairpin ribozyme are found in loop B and include the nucleotides at positions 23 (A20wt→U), 44 (G36wt→A), 46 (A38wt→G) and 47 (U39wt→C). Thus, the cleavage site itself—situated in loop A—remains unchanged. Previous studies on ADHR ribozyme variants showed that the main determinants affecting catalytic activity are the cofactors adenine and divalent magnesium ions.[1]

Several sequential nucleotides and secondary structure motifs in the minimal wt-hairpin ribozyme have been identified to be crucial for its catalysis.[27] Based on studies of the structure–function relationship in the wt-hairpin ribozyme, evaluation of the effect of mutations in ADHR1-nmr compared to the wt-hairpin ribozyme suggests the loss of self-cleavage activity in case of ADHR1 to be a result of the mutation at position 46 (A38wt→G). This assumption is supported by several studies of the wt-hairpin ribozyme that analyze structural and catalytic contributions of the residue A38.[27–30] Replacement of A38 by a guanosine in the wt-hairpin ribozyme, as present in ADHR1-nmr, is reported to result in a 10^4-fold loss of activity.[29] Analysis of the active-site architecture in crystal structures mimicking precatalytic and intermediate states of the wt-hairpin ribozyme revealed that a guanosine at position 38 leads to remarkable effects on local geometry.[30]

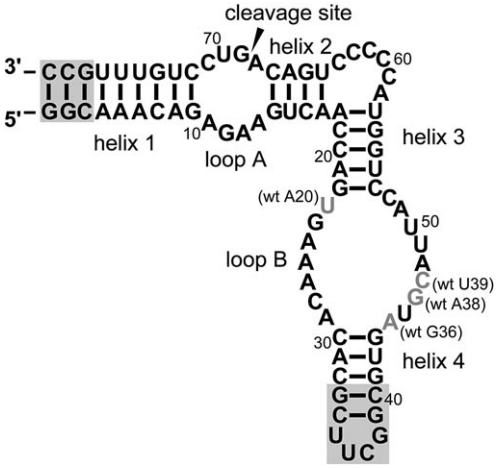

Figure 1. Secondary structure of ADHR1-nmr (helices 1–4, loops A and B), additional base pairs compared to ADHR1[1] are shaded in gray, nucleotides mutated compared to the wt-hairpin ribozyme are highlighted in gray (with annotated mutation and numbering of wt-hairpin ribozyme).

By using NMR spectroscopy, structure and dynamics of RNAs can be depicted. In addition, characterization of RNA conformational transitions and the structural changes due to the addition of cofactors, for example, ions, small molecules or even proteins, could give insight into biomolecular reaction mechanisms.[31,32] Here, we used static and time-resolved NMR spectroscopy to characterize the pre- and postcleaved conformations of the adenine-dependent hairpin ribozyme (ADHR1-nmr) and to monitor cleavage-induced structural changes in real time.

We report here data for the largest RNA for which time-resolved NMR studies could be described thus far. After studies on the minimal hammerhead ribozyme,[33] the studies on ADHR1-nmr represent the second example for which cleavage kinetics catalyzed by RNA ribozymes have been investigated by time-resolved NMR spectroscopy. The NMR-spectroscopic characterization of the pre- and postcleaved conformations of ADHR1-nmr is based on the NMR imino proton resonance assignment prior to and after cleavage, and indicates that structural rearrangements can be detected but are restricted to the vicinity of the cleavage site. Based on ^{31}P NMR spectroscopy, the mechanistic assumption of forming a 2′,3′-cyclic phosphodiester on the 5′-site of the cleaved RNA strand as underlying the catalytic cleavage process could be confirmed. The cleavage rate constants observed following spectral changes of the imino proton resonances over time were found to be on the timescale of minutes. Thus, the reaction is markedly slower than detected for the minimal hammerhead ribozyme.[33] This time scale enabled structural changes due to the cleavage process to be studied by real-time 1D and 2D NMR-spectroscopic methods. The ADHR1-nmr structural transition upon catalysis and the structural impact of the catalytically essential exoge-

nous cofactors Mg^{2+} and adenine on its conformational transition were analyzed, both by biochemical and NMR-spectroscopic methods.

Results

Characterization of the precleaved conformation of the adenine-dependent hairpin ribozyme

The structural characterization of ADHR1-nmr is based on the assignment of the exchangeable imino proton NMR resonances of the 80-nucleotide long RNA. Imino proton signals are direct reporters of base pairing interactions in RNA and their chemical shift is sensitive to structural transitions and changes in intermolecular interactions determined on the level of secondary and tertiary structure.[31] The NMR spectra of ADHR1-nmr strongly support the secondary structure prediction based on the structure model of the minimal hairpin ribozyme domain from the negative RNA strand of the TRSV[18,34] (Figure 1) with respect to number and type of imino proton signals. For ADHR1-nmr, 23 imino proton signals of nucleotides in helical elements are expected, including nine uridine resonances involved in A–U base pairing interactions and 14 guanosine resonances involved in G–C base pairing interactions. In addition, the well-characterized UUCG tetraloop is known to show a guanosine imino proton signal.[35,36]

The imino proton region in the $^{1}H,^{15}N$ HSQC spectrum of the uniformly ^{15}N-labeled adenine-dependent hairpin ribozyme RNA displays 21 resolved signals with homogenous line widths ($I^{-1/2}(^{1}H) \sim 30$ Hz; Table S1 in the Supporting Information). The HNN COSY experiment[37] maps base pairing pattern through scalar couplings between donor and acceptor atoms across each hydrogen bond of type N–H···N. By utilizing information derived from the HNN COSY spectrum of ADHR1-nmr precleavage, all seven detectable uridine signals could be assigned to be involved in A–U base pairing interactions, and 13 detectable guanosine signals to be involved in G–C base pairing interactions. The guanosine imino proton signal in the UUCG-tetraloop capping helix 4 in ADHR1-nmr could be identified by its characteristic proton chemical shift at 9.7 ppm.[35] Thus, based on the secondary structure prediction only two uridine resonances involved in A–U base pairing interactions and one imino proton signal from a G–C base pairing interaction are not detectable by NMR spectroscopy.

However, the RNA secondary structure of the helical elements in ADHR1-nmr is exclusively stabilized by Watson–Crick base pairing motifs. The NMR spectra thus lack advantageous spectral dispersion, typically detected in spectral regions of noncanonical base pairing motifs that can serve as unique assignment starting points. Many of the sequential imino–imino proton connectivities could be resolved in 2D $^{1}H,^{1}H$ NOESY (Figure 2A) and 3D $^{1}H,^{1}H,^{15}N$ NOESY-HSQC spectra. Still, with this sizable RNA, spectral overlap leads to incomplete sequential connectivities and hinders straightforward resonance assignment. To complete the NMR-spectroscopic assignment of the full-length RNA, our strategy included the use of model hairpin RNAs mimicking smaller structural elements of the full-length construct. We utilized mimics of helices 2, 3 and 4 (Figure 2B). Imino proton resonances in helix 1 could be assigned as there is a single sequence of three succeeding A–U base pairing interactions in ADHR1-nmr serving as a unique starting point for the imino proton resonance assignment. The sequential assignment of the model hairpin RNAs was performed by recording 2D $^{1}H,^{1}H$ NOESY and $^{1}H,^{15}N$ HSQC spectra. The assignments of the model hairpin RNAs could then reliably be correlated with the spectra of the full-length ADHR1-nmr RNA (Figure 2B). Both, the imino–imino proton connectivities and the chemical shifts of the signals in the NMR spectra of the

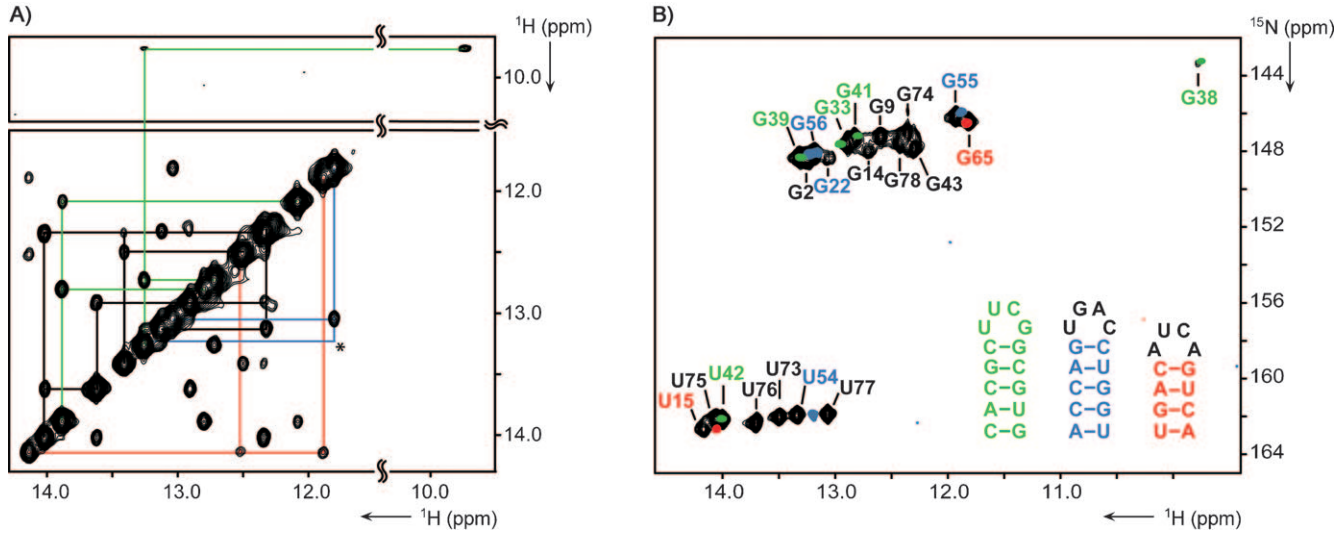

Figure 2. A) $^{1}H,^{1}H$ NOESY spectrum of ADHR1-nmr (293 K, without Mg^{2+}, 600 MHz, 150 ms mixing time); lines represent resolved imino–imino proton connectivities with color coding according to full-length secondary structural elements that are mimicked by model hairpin RNAs; asterisk: NOE detectable in $^{1}H,^{1}H$ NOESY spectrum of ADHR1-nmr with different mixing time; B) overlay of $^{1}H,^{15}N$ HSQC spectra (283 K) of full-length ADHR1-nmr (black) and model hairpin RNAs with annotated resonance assignment of ADHR1-nmr. Model hairpin 1 is color coded in green (mimic of helix 4), model hairpin 2 in blue (mimic of helix 3) and model hairpin 3 in red (mimic of helix 2); inset: secondary structures of model hairpin RNAs.

model hairpin RNAs agree well with the respective corresponding residues in the full-length RNA, and could thus confirm the resonance assignment of ADHR1-nmr (Figure 2) and also the proposed secondary structure. The signals that are missing compared to the secondary structure prediction belong to the terminal base pair of helix 1 (imino proton signal G1) and the closing base pairs of helices 2 and 3 pointing to the connecting C-rich loop (imino proton signals U57 and U64), which are probably in fast exchange with the solvent and therefore not detectable by NMR spectroscopy.

Investigation of the mechanism of catalytic cleavage in the adenine-dependent hairpin ribozyme

In naturally occurring small, self-cleaving ribozymes, including the wt-hairpin ribozyme,[38,39] hydrolysis of the RNA backbone proceeds by a transesterification mechanism that results in the formation of a 2′,3′-cyclic phosphodiester and a 5′-hydroxyl terminus (Figure 3A). The in-line orientation of the reactive centers is the structural prerequisite for the cleavage mechanism to proceed. NMR studies on the isolated domain A show that the RNA nucleotides around the active site adopt A-form conformation,[40] and therefore sample conformations that are not suitable to perform the reaction. In crystal structures of the docked state of a ribozyme–inhibitor complex and a transition-state mimic, nucleotides around the scissile phosphodiester bond were found to adopt a reactive conformation.[28,41]

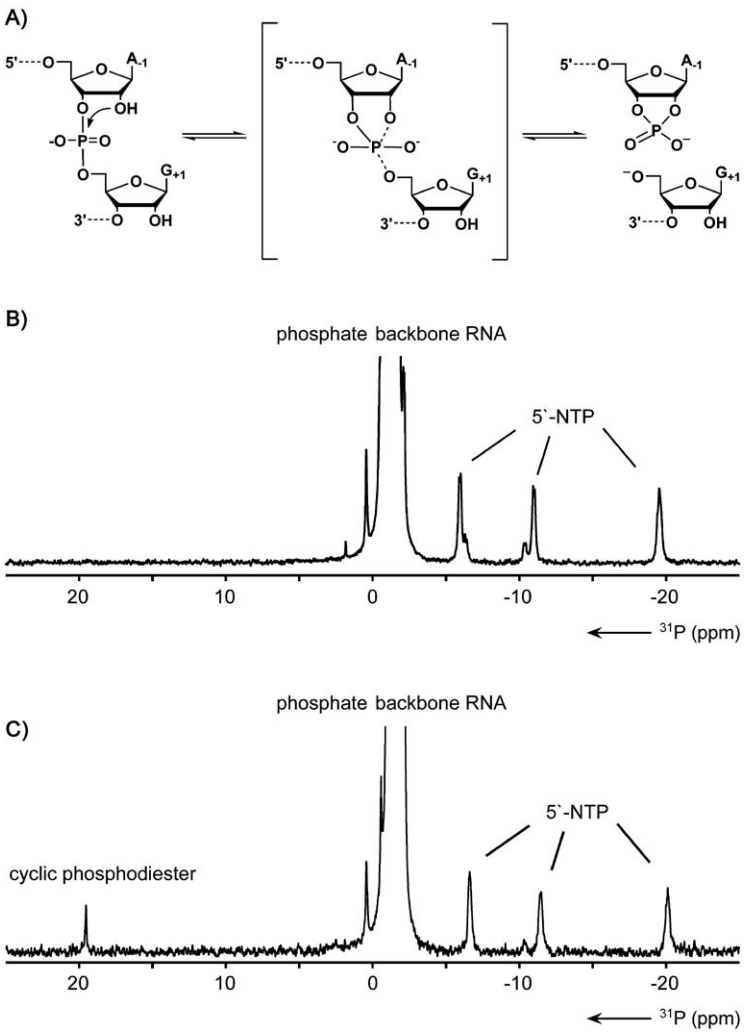

Figure 3. A) Schematic transesterification mechanism; ^{31}P NMR spectra of ADHR1-nmr (298 K, 6 mM Mg^{2+}), B) in the precleaved conformation (absence of adenine), and C) postcleavage, after incubation with adenine for 20 h.

Comparison of ^{31}P NMR spectra of the ADHR1-nmr ribozyme in the pre- and postcleaved conformation shows an additional upcoming signal at 19.5 ppm after cleavage (Figure 3B and C). This ^{31}P chemical shift is indicative of a 2′,3′-cyclic phosphodiester[42] and well-separated from the ^{31}P NMR resonances corresponding to the RNA phosphodiester backbone at approximately −1.5 ppm. Thus, this signal represents a direct reporter of one characteristic cleavage product in the proposed reaction mechanism.

In order to gain insight into RNA conformational changes upon catalysis, we analyzed the imino proton NMR spectra of ADHR1-nmr after catalytic cleavage. The NMR spectra after incubation with adenine reveal significant differences compared to the ones of the RNA prior to cleavage (Figure 4). Biochemical cleavage and ligation studies on ADHR ribozyme variants revealed that the adenine-induced cleavage reaction is reversible.[1] The NMR spectra show that several signals corresponding to the precleaved RNA conformation are detectable in the NMR spectra postcleavage (Figure 4A, indicated with the suffix "-pre"). Analysis of the NMR signals postcleavage shows ~52% signal decay. These results are in agreement with biochemical cleavage studies on ADHR ribozyme variants with which full-length RNA could be detected on denaturing PAGE after 30 h.[1] In addition, the kinetics associated with the cleavage process occurs on a timescale of minutes, which makes the cleavage reaction well-amenable to be studied by real-time NMR-spectroscopic methods. Analysis of the time-resolved NMR studies identifies nine reporter signals for the cleavage process. Most of these imino proton resonances are well-resolved in the 1D imino proton NMR spectra. However, the decaying signal G14 and the upcoming signal for residue G9 in the postcleaved conformation (G9post) could only be resolved in the ^{15}N dimension (Figure 4A). Thus, no kinetic data could be obtained for these residues in the time-resolved 1D NMR experiments. Additional time-resolved 2D NMR spectroscopic[43] studies supported the 1D experiments, albeit with worse signal-to-noise (data not shown). Hence, the following kinetic analysis of the cleavage process is based on the 1D time-resolved NMR studies.

The extracted kinetic traces of the seven residues resolved in the 1D time-resolved NMR experiments show a good signal-to-noise ratio and can reliably be fitted with a monoexponential function. The kinetics observed for all RNA residues reveals comparable time constants (k [min^{-1}]) that are slow on the

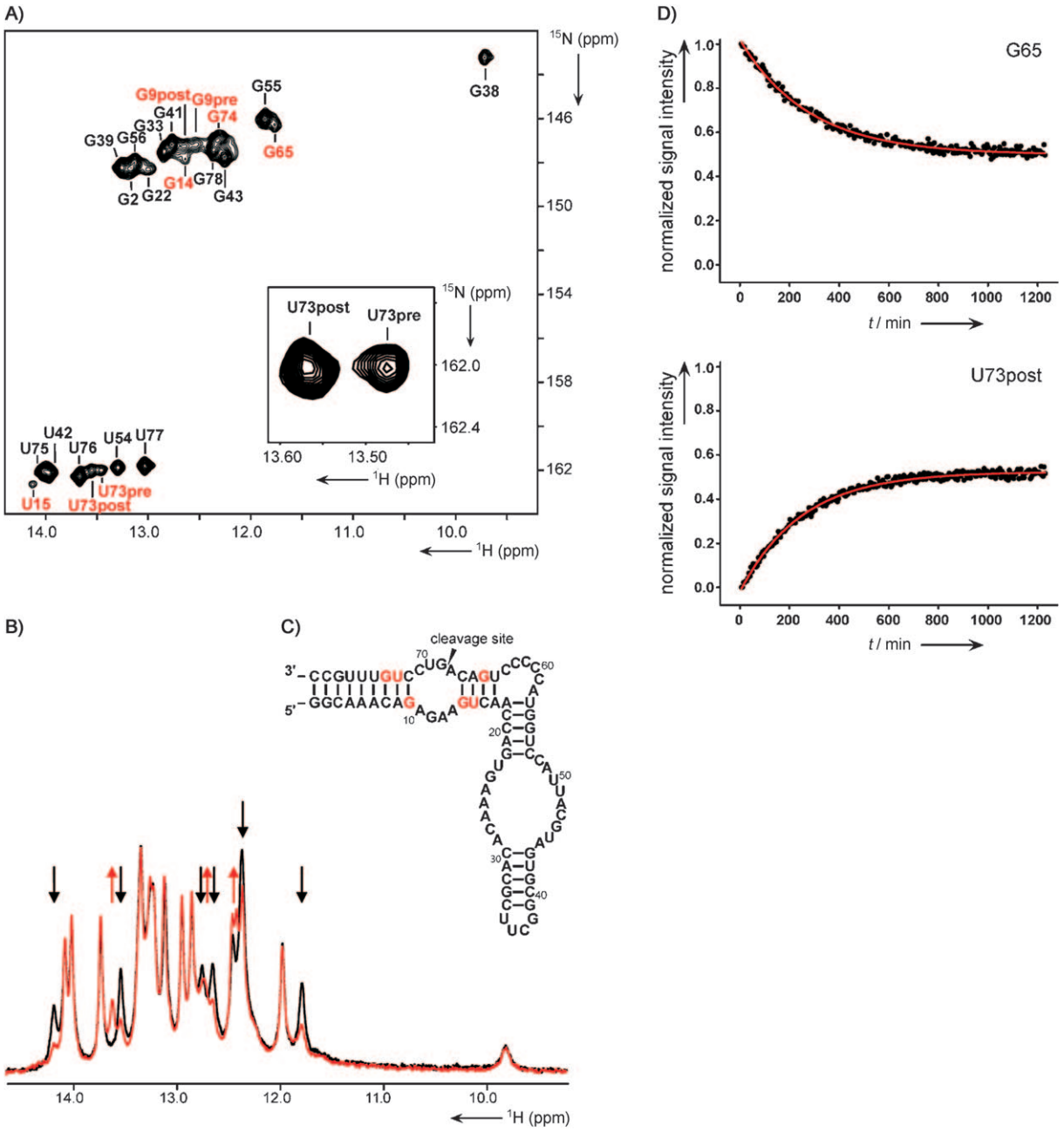

Figure 4. A) $^{1}H,^{15}N$ HSQC spectrum of ADHR1-nmr postcleavage with annotated imino proton resonance assignment; suffixes "-pre" and "-post" indicate resonances present in the respective RNA conformation. Inset: detailed section of imino proton resonances corresponding to U73 in the pre- and postcleaved conformations; B) overlay of 1D imino proton spectra of ADHR1-nmr in the precleaved (without adenine, black) and postcleaved conformations (incubation with adenine for 20 h, red); red arrows indicate upcoming imino proton signals upon cofactor addition, black arrows indicate signals with decreasing intensity upon cofactor addition; C) the secondary structure of ADHR1-nmr; the nucleotides affected upon adenine addition are color coded in red; D) normalized signal intensity versus time (in min) with monoexponential fit (red solid line) of imino proton signals G65 and U73post extracted from 1D time-resolved NMR spectroscopy experiments.

NMR time scale (Figure 4D, Table 1) with individual variations for different residues from the averaged reaction time constant Δk_{mean} below 9%. The half-life of the observed cleavage reaction is about 3 h (averaged reaction half-life $t_{1/2}$ (~187.2 ± 11.1) min). The 5′-cleaved product strand does not dissociate from the ribozyme after cleavage. In fact, only the signals situated in regions around the cleavage site in helices 1 and 2 are affected. However, there are two different cleavage-dependent effects detectable on the imino proton signals of ADHR1-nmr. 1) The imino proton signals G14, U15 and G65 situated in helix 2 strongly decay in intensity; this suggests these base pairing interactions to be absent in the postcleaved conformation. 2) The signals corresponding to nucleotides G9, U73 and G74 also decay in intensity, but in contrast resonate at a different chemical shift in the postcleaved conformation. The chemical-shift difference between the pre- and postcleaved state is more pronounced for G9 and U73 (Figure 4, assignment of signals indicated with suffixes "-pre" and "-post"), while the chem-

Table 1. Kinetic data of adenine-induced ADHR1-nmr cleavage extracted from 1D time-resolved NMR spectroscopy experiment.

Residue	k [min^{-1}]	Δk [min^{-1}]
U15	0.0034	0.50×10^{-4}
G65	0.0036	0.53×10^{-4}
G9pre	0.0039	0.71×10^{-4}
U73pre	0.0036	0.48×10^{-4}
U73post	0.0040	0.52×10^{-4}
G74pre	0.0039	0.71×10^{-4}
G74post	0.0036	0.47×10^{-4}

ical shift difference of G74 pre- and postcleavage is within the line widths of the signals. The neighboring nucleotide in helix 1, U75, is not affected upon cleavage; here, neither chemical shift nor intensity changes are detectable. These results suggest helix 1 to be stable and unaffected in the terminal six base pairs, while there is a conformational change affecting the nucleotides next to loop A. The observed cleavage-dependent effect seen in helices 1 and 2, are likely due to the structural rearrangements in loop A. A structural rearrangement in this region is supposed to be part of the cleavage process as the required in-line conformation of the reactive atoms has to be sampled.

Deciphering contributions of cofactors to catalysis

With its polyanionic character, RNA often requires associated cations to adopt a fully folded and active conformation. Thus, distinguishing between the specific role of cations in RNA catalysis of either stabilizing the functional tertiary fold or participating in catalytic chemistry could be difficult. Using biochemical and NMR-spectroscopic studies, we analyzed the role of Mg^{2+} ions that are known to be essential in catalysis of the adenine-dependent hairpin ribozyme.[1]

If Mg^{2+} ions actively participate in acid/base chemistry of the catalytic reactions, they could either act as: 1) Brönsted acid/base by their complexed hydroxide ions, or as 2) Lewis acid/nucleophile activation through inner-sphere coordination. In order to map out these possibilities, Mg^{2+} ions were replaced by Na^+ ions[44,45] and $[Co(NH_3)_6]^{3+}$ [46] in the cleavage reaction. The latter is known to be a structural analogue of hexahydrated Mg^{2+} with a kinetically stable outer-coordination sphere that associates only through electrostatic and outer sphere hydrogen bonding but induces a comparable RNA structure.

Figure 5 shows the results of the biochemical cleavage studies of ADHR1-nmr in the presence of different cations. Analyzing the cleavage kinetics in the presence of Mg^{2+} (6 mM) by denaturing PAGE and time-resolved NMR spectroscopy indicates the cleavage efficiency of ADHR1-nmr to be ~48%. Albeit with slightly decreased cleavage efficiency, high concentrations of monovalent Na^+ ions (cleavage efficiency ~40%) as well as cobalt hexamine (cleavage efficiency ~30%) both promote the adenine-dependent cleavage reaction. Thus, the possible substitution of Mg^{2+} ions in the cleavage reaction of the adenine-dependent hairpin ribozyme by these two Mg^{2+} analogues excludes the essential need of direct metal coordination to functional groups at the active site to promote chemical catalysis. However, these observations cannot rule out a possible role of Mg^{2+} ions in promoting the catalytic strategy of this ribozyme, as for example, in electrostatic transition state stabilization.[47]

Since Mg^{2+} has previously been shown to be a crucial cofactor in ADHR1-nmr catalysis, we analyzed possible Mg^{2+}-dependent structural effects in the ribozyme by NMR spectroscopy. Interactions of metal ions with the RNA might induce chemical shift perturbations (CSP) of those resonances that are involved in or are in close proximity to Mg^{2+} binding sites. In addition, the formation or rearrangement of secondary or tertiary structural elements might result in changes of NMR-spectroscopic characteristics, as for example, the detection of additional or disappearance of signals or the changes in structural connectivities as evidenced by additional or missing NOE connectivities. Here, we used imino proton resonances as NMR-spectroscopic reporter signals as done in previous analysis[48–50] to identify Mg^{2+}-dependent structural effects in ADHR1-nmr. Direct comparison of the NMR spectra ($^1H,^{15}N$ HSQC, $^1H,^1H$ NOESY) in the absence of Mg^{2+} and upon titration with Mg^{2+} shows chemical-shift changes for a number of imino proton resonances. However, changes in tertiary structure that could be detected in $^1H,^1H$ NOESY spectra displaying HH distances were not observed (data not shown). Furthermore, no additional imino proton signals appear in the presence of Mg^{2+}. These observations imply that the secondary structural elements are already preformed and stable without magnesium. However, titration of the RNA with Mg^{2+} reveals chemical-shift changes of various imino proton signals and indicates Mg^{2+} binding sites in the millimolar range, which are located

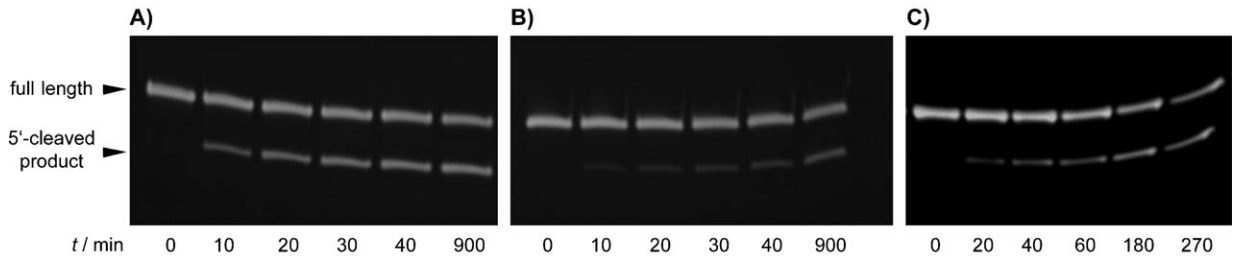

Figure 5. Adenine-induced cleavage reaction of ADHR1-nmr analyzed on denaturing PAGE (10%) in the presence of: A) 6 mM $MgCl_2$, B) 24 mM $[Co(NH_3)_6]Cl_3$, and C) 4 M NaCl.

in all four helical elements of the RNA (Figures 6 and 7). The NMR-spectroscopic studies therefore support the notion that Mg^{2+} stabilizes the correct fold of the RNA by unspecific electrostatic interactions that are crucial to the formation of an active RNA conformation.

In contrast to the catalytic activity in the wt-hairpin ribozyme, ADHR1-nmr is only active in the presence of the cofactor adenine. The rescue of activity by the exogenous nucleobase might either be due to stabilization of active-site architecture or due to direct participation in catalytic chemistry. We investigated the role of adenine in the cleavage reaction by NMR spectroscopy using unlabeled ADHR1-nmr RNA and ^{13}C,^{15}N-labeled adenine. The use of an analogous labeling scheme turned out to be an effective tool in NMR studies of RNA–ligand interactions, for example, in case of riboswitch RNAs in order to assign specific binding of small ligands to RNA,[51] or even to detect the presence of low-affinity initial encounter complexes of RNA and ligand.[52] In addition, pH-dependent chemical shift information in ^{13}C NMR experiments are reported to be useful tools for studying the protonation state of individual nucleotides in RNA.[53]

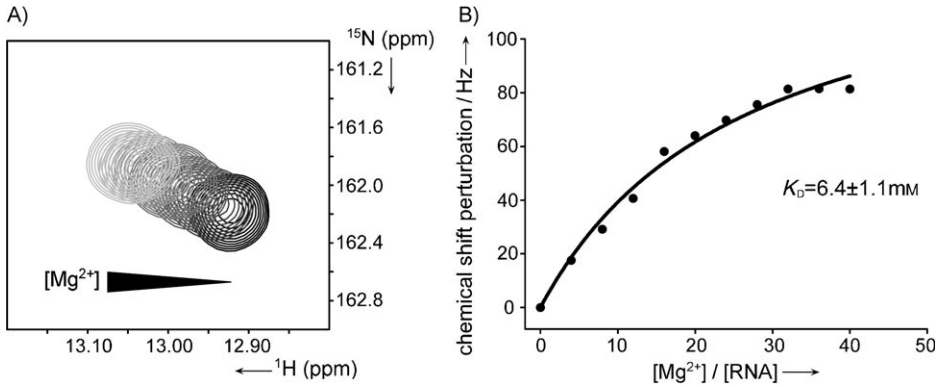

Figure 6. Chemical-shift perturbation of imino proton signal U77 upon Mg^{2+} titration (0–10 mM); A) overlay of ^{1}H,^{15}N HSQC spectra; B) correlation of chemical-shift perturbation [Hz] as a function of $[Mg^{2+}]$/[RNA] ratio resulting in a $K_D[Mg^{2+}]$ value of (6.4 ± 1.1) mM.

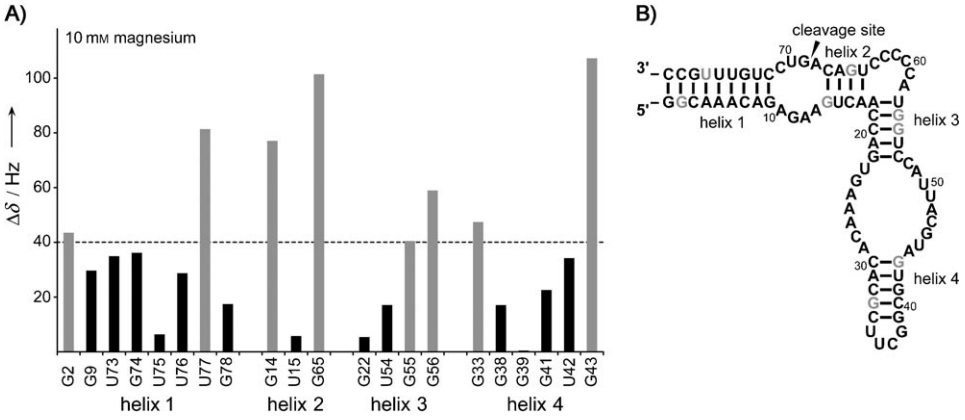

Figure 7. A) Chemical-shift perturbation $\Delta\delta$ [Hz] of ADHR1-nmr imino proton resonances; B) signals that show $\Delta\delta$ values > 40 Hz are highlighted in gray on the secondary structure of ADHR1-nmr.

The NMR spectroscopic experiments were performed with RNA:adenine ratios of 5:1 and 1:1, and in order to investigate possible interactions at conditions in which catalytic activity is observed, possible adenine–RNA interactions were also investigated at a ~25-fold excess of ligand over RNA. Although the mentioned labeling scheme would enable the determination of various ligand functional groups (N9–H9, $-NH_2$, C2–H2, C8–H8) in binding, for each RNA:adenine ratio even in the presence of excess RNA (5:1), only NMR resonances of the free form of the ligand could be detected. Neither chemical-shift changes nor additional signals due to specific binding to the RNA or a different protonation state of the cofactor during reaction could be observed in ^{1}H,^{15}N HSQC and ^{1}H,^{13}C HSQC spectra (Figure 8). In addition, analysis of NMR line widths of nonexchangeable ligand signals (C2–H2 and C8–H8) and the adenine amino signal only shows minor changes in the presence of ADHR1-nmr (data not shown) and therefore does not report on the timescale of protonation or support unspecific binding of the ligand to the RNA.

Discussion

Key questions in understanding catalysis in the adenine-dependent hairpin ribozyme representing a model for which ribozyme-mediated RNA catalysis is ligand induced, include resolving how catalytic activity is realized and which structural rearrangements are associated with the cleavage process.

By using static and time-resolved NMR-spectroscopic methods, deciphering of structural changes and observation of conformational transitions at atomic resolution is feasible. Prerequisite therefore is the resonance assignment of the RNA. With its 80 nucleotides, ADHR1-nmr represents a large RNA for NMR-spectroscopic studies. The approach successfully applied here, consists of dividing the molecule into smaller structural fragments that can then be analyzed separately. Correlation of the chemical shifts and NOE connectivities of the model hairpin RNAs with the full-length RNA construct allowed us to complete the imino proton resonance assignment of ADHR1-nmr. Based on the assignment of the pre- and postcleaved conformations of ADHR1-nmr, the ligand-induced catalytic mechanism could be analyzed.

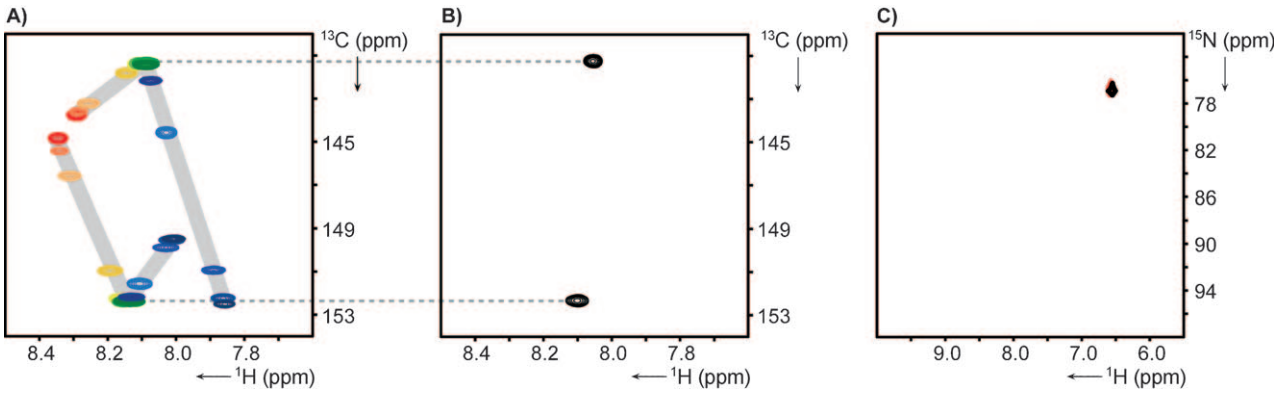

Figure 8. A) Overlay of ^{1}H,^{13}C HSQC spectra (298 K, 600 MHz) from pH titration of ^{13}C,^{15}N-labeled adenine (color coding according to pH, red: 1.8, green: 7.5, dark blue: 13); B) ^{1}H,^{13}C HSQC spectrum of ^{13}C,^{15}N-labeled adenine in the presence of ADHR1-nmr (298 K, without Mg^{2+}, 600 MHz); C) overlay of amino resonance region of ^{1}H,^{15}N HSQC spectra of ^{13}C,^{15}N-labeled adenine (red) and ^{13}C,^{15}N-labeled adenine in the presence (black) of ADHR1-nmr (without Mg^{2+}).

Several factors can in principle contribute to reaching catalytic activity in ADHR1-nmr, including: 1) substrate alignment, 2) activation of the nucleophile/protonation of the leaving group (acid/base chemistry), and 3) transition-state stabilization/ground-state destabilization.

1) The reported local A-form geometry of the active site in the wt-hairpin ribozyme[40] is not the reactive conformation required for phosphodiester hydrolysis in an S_N2 reaction. Also, in the adenine-dependent hairpin ribozyme, all NMR spectroscopic data support A-form geometry in the ground-state conformation. Thus, the local conformation has to be altered to result in an active conformation, albeit we provide evidence that this conformation is sampled only transiently.
2) Various ribozyme functional groups are candidates for proton transfer in acid/base chemistry. In addition, exogenous Mg^{2+}, or in case of ADHR1-nmr even the cofactor adenine can exert this function.
3) Rupert et al. have reported on crystal structures of the wt-hairpin ribozyme in its precleaved state, of a transition-state mimic, and its postcleaved state.[28] From the comparison of the active-site structures and hydrogen-bonding interactions in the three states, transition-state stabilization is likely to contribute to catalytic efficiency.

The ^{31}P NMR signal detected for the adenine-dependent hairpin ribozyme after cleavage with a characteristic chemical shift at 19.5 ppm can be assigned to a cyclic phosphodiester. Thus, the data are consistent with specific cleavage of a phosphodiester bond also for the adenine-dependent hairpin ribozyme. Due to sequence homology, the conformation around the active site in ADHR1-nmr is likely to be similar to the reported solution NMR structure of the isolated domain A of the wt-hairpin ribozyme.[40] The observation that the NOE connectivities and the chemical shifts of ADHR1-nmr resonances are in complete agreement with signals of the model hairpin RNAs suggests that the helical elements in ADHR1-nmr are present in an A-form conformation and are not involved in additional tertiary interactions. The ground state of ADHR1-nmr detected in solution thus samples a conformation incompetent for phosphodiester hydrolysis. Hence, addition of the cofactor adenine transiently aligns the active-site residues in the adenine-dependent hairpin ribozyme and might participate in transition-state stabilization.

Analysis of the imino proton resonances in the static and time-resolved NMR spectra provides further insight into different mechanistic aspects of catalysis in the adenine-dependent hairpin ribozyme. As stated above, cleavage of the RNA phosphodiester backbone can directly be detected by ^{31}P NMR spectroscopy. In addition, comparison of NMR spectra pre- and postcleavage indicates that the 5′-cleaved product RNA strand remains associated with the ribozyme and does not support product dissociation as part of ribozyme kinetics. Indeed, apart from signals G9, U73 and G74, resonances corresponding to nucleotides in helix 1 are unaffected upon cleavage. Thus, the stabilizing effect of the six terminal Watson–Crick base pairs in helix 1 in the product state might not be overcome by the adenine-dependent hairpin ribozyme. Thus, the time-resolved NMR spectroscopic experiments exclusively report on RNA cleavage (Scheme 1). However, cleavage-dependent kinetics can be observed for resonances corresponding to nucleotides situated in helices 1 and 2 around the active site of ADHR1-nmr. The kinetics of ADHR ribozyme activity have been shown to be dependent on the RNA:adenine ratio.[1] Under the conditions employed in the time-resolved NMR studies, a ~25-fold excess of ligand over RNA was used and cleavage took place on a timescale of minutes (averaged reaction half-life $t_{1/2}$ (~187.2±11.1) min). The kinetic behavior could be analyzed by a monoexponential fitting function; this suggests the reaction to be a first-order kinetic process. In addition, the cleavage process follows a concerted mechanism since all imino proton reporter signals show similar time-dependent properties.

Ribozyme kinetics reports on an underlying reaction mechanism in which equilibrium is reached between cleavage and product dissociation and the reverse reaction, namely product association and ligation (Scheme 1). Analysis of cleavage and ligation indicates the reversibility of the reaction and shows no complete conversion to the respective complementary state of the ADHR ribozyme as evidenced by denaturing PAGE.[1] Al-

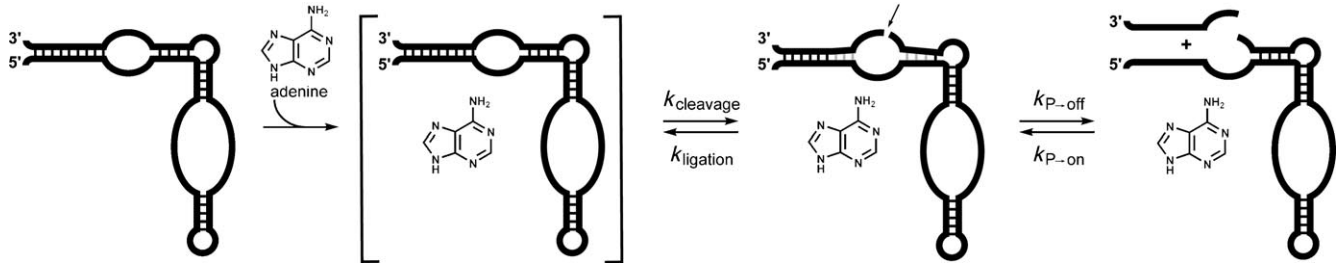

Scheme 1. Schematic representation of the kinetic model of adenine-dependent hairpin ribozyme activity. Product dissociation is not detectable in the NMR spectra of ADHR1-nmr (P→off: product dissociation, P→on: product association).

though the NMR studies focused on the cleavage reaction, this observation is consistent. The NMR spectra postcleavage still show signals corresponding to the RNA in its precleaved conformation. Thus both, biochemical and NMR-spectroscopic studies report on the kinetics that reflects equilibrium between cleavage and ligation.

In case of the wt-hairpin ribozyme, the participation of ribozyme functional groups in acid/base chemistry or in transition-state stabilization has been suggested. Proposed candidates are nucleotides situated in the active site loop A and nucleotides in loop B. The latter are involved in a docking interaction[24] that is reported to be a crucial prerequisite for catalysis. The crystal structure of a ribozyme–inhibitor complex supports this hypothesis and indicates several interdomain tertiary contacts, including an interdomain Watson–Crick interaction.[41] Catalysis in the minimal hairpin ribozyme was found to proceed through a multistep reaction pathway for which the rate constants for individual conformational transitions could be determined, including rate constants for docking and undocking kinetics. Here, the docked state was found to be stable enough so that the internal equilibrium between cleavage and ligation was reached before undocking occurred.[54–56]

Based on the imino proton resonances, our NMR studies do not indicate a stably docked intermediate RNA conformation during ADHR1-nmr catalysis in solution. Neither in the precleaved nor in the product state, or when chemical shifts were used as very sensitive reporters for changes in the local environment, could an interdomain Watson–Crick interaction be detected even in the presence of Mg^{2+} (and absence of cofactor adenine). The imino proton resonances of ADHR1-nmr in the presence and absence of the cofactors show homogenous line widths and especially signals from helices 3 and 4 do not show any changes in the different states, neither in intensity nor in chemical shift. However, we cannot exclude potential interdomain docking as part of the catalytic mechanism in ADHR1-nmr. Still, the lack of additional imino proton signals corresponding to a stable alternate conformation, as for example, observed for a structural rearrangement in the guanine-sensing riboswitch aptamer domain[52] suggests that potential interdomain interactions in the adenine-dependent hairpin ribozyme are likely to be too transient to induce detectable changes in the average structure of the RNA on the time scale of our NMR spectroscopic experiments.

The catalytic activity of ADHR, the cleavage and ligation reactions, depend on the concentration of the cofactor adenine as well as on Mg^{2+}.[1] NMR spectroscopic Mg^{2+} titration of ADHR1-nmr revealed Mg^{2+} binding sites in the millimolar range for nucleotides situated in all four helical elements. The $K_D[Mg^{2+}]$ for the imino proton signal U77, for example, is determined to be (6.4 ± 1.1) mM. ADHR1-nmr is catalytically active in the presence of high concentrations of monovalent salt (4 M Na^+) or of the magnesium analogue cobalt hexamine (24 mM). These observations suggest that direct metal contacts to functional groups in the active site of ADHR1-nmr are not obligatory for catalytic chemistry. However, Mg^{2+} might stabilize the ground-state and transition-state structures of the ADHR ribozyme by unspecific electrostatic interactions as a prerequisite for preorganization of functional elements or compensation of negative charge repulsion.

Nucleobases G8 and A38 are situated near the active phosphodiester bond in the crystal structures of the wt-hairpin ribozyme and their mutation or abasic substitution leads to severe loss of activity; this confirms their relevance in catalysis.[16,29,57] Assuming that substitution of the nucleotide at position 38 in the wt-hairpin ribozyme (A38wt) by a guanosine in ADHR1-nmr is crucial for the loss of activity, the nucleobase that restores activity could overtake the function of A38wt in catalysis. However, neither specific ligand binding nor a low-affinity RNA–ligand complex could be detected by NMR spectroscopy. Thus, the interaction of the ribozyme with the cofactor has to be transient and too weak to significantly change the structure of the RNA or to modulate the spectroscopic characteristics of the cofactor.

We conclude that in the adenine-dependent hairpin ribozyme the barriers towards the transition state are significantly higher than in the wt-hairpin ribozyme, in line with compromised catalytic activity. Single-molecule fluorescence studies on group II intron ribozymes revealed an only transiently populated on-pathway kinetic intermediate.[58] Analogously, we propose a catalytic mechanism for ADHR1-nmr, in which the active conformation is only infrequently reached, but once it is established, catalytic chemistry can proceed. Conformational dynamics and activation of the RNA ground-state population rather than chemistry of catalysis define the rate-limiting step in RNA cleavage and ligation catalyzed by ADHR1-nmr.

The starting conformation of ADHR1-nmr shows homogenous line widths for nucleotides in the helical elements but is not yet catalytically reactive. Although structural changes detected on our reporter signals are only minor, the catalytically reactive conformation has to be induced by metal ions. The

catalytic reaction itself—namely the mechanism of RNA phosphodiester backbone cleavage—is identical to that of the wt-hairpin ribozyme. However, in contrast to the wt-hairpin ribozyme, an additional cofactor is essential to result in catalytic activity. Thus, the underlying chemistry of the reaction in ADHR1-nmr still depends on an exogenous and potential prebiotic cofactor that might have been displaced by the ribozyme itself, namely ribozyme functional groups. Regarding the efficiency and the rate acceleration of the reaction such conceived order of events might be correct since the ADHR ribozyme is inferior as catalyst in both aspects when compared to the wt-hairpin ribozyme and even more so when compared to protein ribonucleases. The exogenous cofactor adenine is able to overtake essential functional properties in catalysis. Studying the adenine-dependent hairpin ribozyme therefore enables the dissection of catalytic contributions to ribozyme activity and represents a model for evolutionary ancestors of chemistry essential for life, and thus, might provide insight into cellular catalysis in an "RNA world".

Experimental Section

RNA and ligand synthesis: ADHR1-nmr was produced by T7 RNA polymerase in vitro transcription with unlabeled rNTPs (Fermentas, St. Leon-Rot, Germany) or ^{15}N-labeled rNTPs (Silantes, Munich, Germany). The RNA was purified by electrophoresis on denaturing polyacrylamide gels. After elution from the gel by diffusion, ADHR1-nmr was recovered by ethanol precipitation. Unlabeled model hairpin RNA constructs were purchased from Dharmacon (Boulder, CO, USA). RNA buffer conditions for the NMR spectroscopic studies were HEPES (40 mM), pH ~7.5, $MgCl_2$ (6 mM) if not otherwise stated. ^{13}C,^{15}N-labeled adenine was synthesized as described before.[51]

Cleavage reactions on denaturing PAGE: Adenine-induced cleavage of ADHR1-nmr was followed by kinetic studies in the presence of different salts: $MgCl_2$, NaCl or $[Co(NH_3)_6]Cl_3$. The RNA (20 μM in 40 mM HEPES, pH ~7.5) was firstly folded by a denaturation/renaturation step (90 °C for 1 min and cooled to 23 °C at 3 °C min^{-1}). Then the respective salt $MgCl_2$ (6 mM), NaCl (4 M), or $[Co(NH_3)_6]Cl_3$ (24 mM) was added, and the reaction was started by the addition of adenine (4 mM); concentrations are final concentrations in the complete mixture containing 1 μM RNA and 40 mM HEPES, pH ~7.5. Samples were taken as a function of time; the reaction was blocked by addition of one volume of stop solution (30 mM EDTA, 80% formamide, 0.012% xylene cyanol) and then cooled. Cleavage was analyzed by electrophoresis on denaturing polyacrylamide gels (10%). After migration, RNA was stained with ethidium bromide, visualized with UV, and quantified with the NIH software.

NMR spectroscopy: The NMR experiments were performed by using Bruker NMR spectrometers AV900 MHz, AV800 MHz, AV700 MHz and AV600 MHz with 5 mm *z*-axis gradient TXI-HCN cryogenic probes and a DRX600 MHz spectrometer equipped with a 5 mm *x*,*y*,*z*-axis gradient TXI-HCN-RT probe. The ^{31}P NMR spectra were recorded by using an AV600 MHz Bruker NMR spectrometer with a 5 mm *z*-axis gradient TCI-HCP cryogenic probe and an AV300 MHz Bruker NMR spectrometer equipped with a 5 mm *z*-axis gradient BBO-RT probe.

All NMR spectra were recorded in H_2O/D_2O (9:1) or D_2O by using standard pulse sequences (^{1}H,^{15}N HSQC, ^{1}H,^{13}C HSQC, 2D ^{1}H,^{1}H NOESY, HNN COSY and 3D ^{1}H,^{1}H,^{15}N NOESY-HSQC) with WATERGATE water suppression[59] or jump–return–echo pulse sequences.[60]

Time-resolved NMR spectroscopy experiments: Kinetic 1D NMR experiments were performed by using the following experimental conditions: ADHR1-nmr (220 μM), adenine (5.6 mM), HEPES (40 mM, pH ~7.5), Mg^{2+} (6 mM), 298 K. The data were recorded as pseudo-2D experiments with a time resolution of 4.25 min per 1D spectrum (128 scans each 1D spectrum). The ligand was added manually, which resulted in a reaction dead time of ~2 min. The NMR data were analyzed by using the software TOPSPIN 2.1 and SigmaPlot 11.0. The time constants k [min^{-1}] of upcoming/decaying RNA signals were obtained, extracting their intensities over the reaction time. The data were corrected by the zero point of the kinetics, normalized by the averaged values of the last 20 residual data points and fitted with a monoexponential function. Half-life values ($t_{1/2}$ in min) could be obtained by using the formula for a first-order process: $t_{1/2} = \ln 2/k$. The error stated for k is the fitting error.

Determination of NMR line widths: The NMR line width experiments were performed by using RNA:adenine ratios of 5:1, 1:1 or 1:25. The line widths of ligand signals were extracted from the appropriately zero-filled 2D NMR spectra (^{1}H,^{13}C HSQC or ^{1}H,^{15}N HSQC) and analyzed by deconvolution by using the software TOPSPIN 2.1.

Determination of Mg^{2+}-binding sites and affinities: The chemical-shift perturbations (CSP) $\Delta\delta$ [Hz] of the imino proton signals were determined from ^{1}H,^{15}N HSQC spectra (800 MHz, 293 K) at various Mg^{2+} concentrations. Aliquots from a $MgCl_2$ solution were added, and the Mg^{2+} concentration was increased stepwise in the NMR sample from 0 mM to 10 mM in 1 mM increments. The CSP were calculated for all imino proton signals according to $\Delta\delta = \sqrt{([(\Delta H_N)^2 + (\Delta N/5)^2]/2)}$. Nonlinear regression of the correlation of CSP with the corresponding $[Mg^{2+}]/[RNA]$ ratio resulted in estimation of the dissociation constant (K_D). The K_D was exemplarily analyzed for imino proton signal U77 according to the fitting function: $f(x) = b/2((x+1+a) - \sqrt{((x+1+a)^2 - 4x)})$, where $f(x)$ is the CSP at the respective x; x is the $[Mg^{2+}]/[RNA]$ ratio; a is the ratio of the dissociation constant to [RNA]; and b is the CSP for infinite $[Mg^{2+}]$.[61]

Acknowledgements

The work was supported by the DFG (Deutsche Forschungsgemeinschaft, SFB 579: "RNA–Ligand Interaction" and "Cluster of Excellence: Macromolecular Complexes"), the E.U. ("EU-NMR-European Network of Research Infrastructures for Providing Access & Technological Advancement in Bio-NMR", FP-2005-RII3 contract no.: 026145), the state of Hesse (Center for Biomolecular Magnetic Resonance (BMRZ)) and CNES (Centre National d'Etude Spatiale) and OPV (a specific program of CNRS: Origine des Planètes et de la Vie). We thank Dr. Guy Hervé for valuable discussions.

Keywords: NMR spectroscopy · ribozymes · RNA catalysis · RNA structures · time-resolved NMR spectroscopy

[1] M. Meli, J. Vergne, M. C. Maurel, *J. Biol. Chem.* **2003**, *278*, 9835–9842.
[2] C. R. Woese, *Proc. Natl. Acad. Sci. USA* **1965**, *54*, 1546–1552.
[3] F. H. Crick, *J. Mol. Biol.* **1968**, *38*, 367–379.
[4] L. E. Orgel, *J. Mol. Biol.* **1968**, *38*, 381–393.
[5] W. Gilbert, *Nature* **1986**, *319*, 618.
[6] D. J. Klein, A. R. Ferre-D'Amare, *Science* **2006**, *313*, 1752–1756.

[7] J. C. Cochrane, S. V. Lipchock, K. D. Smith, S. A. Strobel, *Biochemistry* **2009**, *48*, 3239–3246.
[8] W. C. Winkler, A. Nahvi, A. Roth, J. A. Collins, R. R. Breaker, *Nature* **2004**, *428*, 281–286.
[9] R. T. Raines, *Chem. Rev.* **1998**, *98*, 1045–1066.
[10] A. C. Forster, R. H. Symons, *Cell* **1987**, *50*, 9–16.
[11] G. A. Prody, J. T. Bakos, J. M. Buzayan, I. R. Schneider, G. Bruening, *Science* **1986**, *231*, 1577–1580.
[12] M. D. Been, G. S. Wickham, *Eur. J. Biochem.* **1997**, *247*, 741–753.
[13] H. N. Wu, Y. J. Lin, F. P. Lin, S. Makino, M. F. Chang, M. M. Lai, *Proc. Natl. Acad. Sci. USA* **1989**, *86*, 1831–1835.
[14] D. M. Lilley, *RNA* **2004**, *10*, 151–158.
[15] B. J. Saville, R. A. Collins, *Cell* **1990**, *61*, 685–696.
[16] M. J. Fedor, *J. Mol. Biol.* **2000**, *297*, 269–291.
[17] P. A. Feldstein, J. M. Buzayan, G. Bruening, *Gene* **1989**, *82*, 53–61.
[18] A. Hampel, R. Tritz, *Biochemistry* **1989**, *28*, 4929–4933.
[19] J. Haseloff, W. L. Gerlach, *Gene* **1989**, *82*, 43–52.
[20] J. C. Cochrane, S. A. Strobel, *Acc. Chem. Res.* **2008**, *41*, 1027–1035.
[21] P. C. Bevilacqua, R. Yajima, *Curr. Opin. Chem. Biol.* **2006**, *10*, 455–464.
[22] S. Nakano, D. M. Chadalavada, P. C. Bevilacqua, *Science* **2000**, *287*, 1493–1497.
[23] J. A. Esteban, A. R. Banerjee, J. M. Burke, *J. Biol. Chem.* **1997**, *272*, 13629–13639.
[24] N. G. Walter, K. J. Hampel, K. M. Brown, J. M. Burke, *EMBO J.* **1998**, *17*, 2378–2391.
[25] A. Kun, M.-C. Maurel, M. Santos, E. Szathmary in *The Aptamer Handbook: Functional Oligonucleotides and their Applications* (Ed.: S. Klussmann), Wiley-VCH, Weinheim, **2006**, 54–95.
[26] M. Mandal, R. R. Breaker, *Nat. Struct. Mol. Biol.* **2004**, *11*, 29–35.
[27] A. Berzal-Herranz, S. Joseph, B. M. Chowrira, S. E. Butcher, J. M. Burke, *EMBO J.* **1993**, *12*, 2567–2573.
[28] P. B. Rupert, A. P. Massey, S. T. Sigurdsson, A. R. Ferre-D'Amare, *Science* **2002**, *298*, 1421–1424.
[29] Y. I. Kuzmin, C. P. Da Costa, J. W. Cottrell, M. J. Fedor, *J. Mol. Biol.* **2005**, *349*, 989–1010.
[30] C. MacElrevey, J. D. Salter, J. Krucinska, J. E. Wedekind, *RNA* **2008**, *14*, 1600–1616.
[31] B. Fürtig, C. Richter, J. Wöhnert, H. Schwalbe, *ChemBioChem* **2003**, *4*, 936–962.
[32] B. Fürtig, J. Buck, V. Manoharan, W. Bermel, A. Jaschke, P. Wenter, S. Pitsch, H. Schwalbe, *Biopolymers* **2007**, *86*, 360–383.
[33] B. Fürtig, C. Richter, P. Schell, P. Wenter, S. Pitsch, H. Schwalbe, *RNA Biol.* **2008**, *5*, 41–48.
[34] S. E. Butcher, J. M. Burke, *J. Mol. Biol.* **1994**, *244*, 52–63.
[35] B. Fürtig, C. Richter, W. Bermel, H. Schwalbe, *J. Biomol. NMR* **2004**, *28*, 69–79.
[36] C. Cheong, G. Varani, I. Tinoco, Jr., *Nature* **1990**, *346*, 680–682.
[37] A. J. Dingley, S. Grzesiek, *J. Am. Chem. Soc.* **1998**, *120*, 8293–8297.
[38] M. J. Fedor, *Biochem. Soc. Trans.* **2002**, *30*, 1109–1115.
[39] A. R. Ferré-D'Amaré, P. B. Rupert, *Biochem. Soc. Trans.* **2002**, *30*, 1105–1109.
[40] Z. Cai, I. Tinoco, Jr., *Biochemistry* **1996**, *35*, 6026–6036.
[41] P. B. Rupert, A. R. Ferre-D'Amare, *Nature* **2001**, *410*, 780–786.
[42] D. G. Gorenstein, *Annu. Rev. Biophys. Bioeng.* **1981**, *10*, 355–386.
[43] P. Schanda, E. Kupce, B. Brutscher, *J. Biomol. NMR* **2005**, *33*, 199–211.
[44] J. B. Murray, A. A. Seyhan, N. G. Walter, J. M. Burke, W. G. Scott, *Chem. Biol.* **1998**, *5*, 587–595.
[45] A. Hampel, J. A. Cowan, *Chem. Biol.* **1997**, *4*, 513–517.
[46] J. A. Cowan, *J. Inorg. Biochem.* **1993**, *49*, 171–175.
[47] R. K. Sigel, A. M. Pyle, *Chem. Rev.* **2007**, *107*, 97–113.
[48] J. Noeske, H. Schwalbe, J. Wöhnert, *Nucleic Acids Res.* **2007**, *35*, 5262–5273.
[49] M. Schmitz, I. Tinoco, Jr., *RNA* **2000**, *6*, 1212–1225.
[50] Y. Tanaka, T. Hori, M. Tagaya, T. Sakamoto, Y. Kurihara, M. Katahira, S. Uesugi, *Nucleic Acids Res.* **2002**, *30*, 766–774.
[51] J. Noeske, C. Richter, M. A. Grundl, H. R. Nasiri, H. Schwalbe, J. Wöhnert, *Proc. Natl. Acad. Sci. USA* **2005**, *102*, 1372–1377.
[52] J. Buck, B. Fürtig, J. Noeske, J. Wöhnert, H. Schwalbe, *Proc. Natl. Acad. Sci. USA* **2007**, *104*, 15699–15704.
[53] P. Legault, A. Pardi, *J. Am. Chem. Soc.* **1997**, *119*, 6621–6628.
[54] G. Bokinsky, D. Rueda, V. K. Misra, M. M. Rhodes, A. Gordus, H. P. Babcock, N. G. Walter, X. Zhuang, *Proc. Natl. Acad. Sci. USA* **2003**, *100*, 9302–9307.
[55] S. Liu, G. Bokinsky, N. G. Walter, X. Zhuang, *Proc. Natl. Acad. Sci. USA* **2007**, *104*, 12634–12639.
[56] X. Zhuang, H. Kim, M. J. Pereira, H. P. Babcock, N. G. Walter, S. Chu, *Science* **2002**, *296*, 1473–1476.
[57] L. L. Lebruska, I. I. Kuzmine, M. J. Fedor, *Chem. Biol.* **2002**, *9*, 465–473.
[58] M. Steiner, K. S. Karunatilaka, R. K. Sigel, D. Rueda, *Proc. Natl. Acad. Sci. USA* **2008**, *105*, 13853–13858.
[59] M. Liu, X. Mao, C. Ye, H. Huang, J. K. Nicholson, J. C. Lindon, *J. Magn. Reson.* **1998**, *132*, 125–129.
[60] V. Sklenár, A. Bax, *J. Magn. Reson.* **1987**, *75*, 378–383.
[61] R. S. Kang, C. M. Daniels, S. A. Francis, S. C. Shih, W. J. Salerno, L. Hicke, I. Radhakrishnan, *Cell* **2003**, *113*, 621–630.

Received: April 1, 2009
Published online on ■■ ■■, 2009

J. Buck, Y.-L. Li, C. Richter, J. Vergne, M.-C. Maurel, H. Schwalbe**

■■ – ■■

NMR Spectroscopic Characterization of the Adenine-Dependent Hairpin Ribozyme

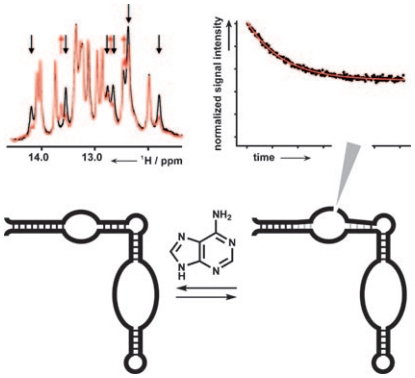

Cut'n'paste: The structural characterization of the pre- and postcleaved conformations and the catalytic activity of a SELEX-derived 80 nucleotide ribozyme RNA, the adenine-dependent hairpin ribozyme (see figure), were carried out by static and time-resolved NMR spectroscopy experiments. The roles of the catalytically essential exogenous cofactors Mg^{2+} and adenine were analyzed by biochemical and NMR-spectroscopic methods.

